Accelerated start-up and improved performance of wastewater microbial fuel cells in four circuit modes: Role of anodic potential

Zhenxing Ren, Guixia Ji, Hongbo Liu, Ming Yang, Suyun Xu, Mengting Ye, Eric Lichtfouse

Journal of Power Sources 535 (2022) 231403

https://doi.org/10.1016/j.jpowsour.2022.231403

Accelerated start-up and improved performance of wastewater microbial fuel cells in four circuit modes: Role of anodic potential

Zhenxing Ren [a,1], Guixia Ji [a,1], Hongbo Liu [a,*], Ming Yang [b], Suyun Xu [a], Mengting Ye [a], Eric Lichtfouse [c]

[a] School of Environment and Architecture, University of Shanghai for Science and Technology, 516 Jungong Road, 200093, Shanghai, China
[b] Chongqing New World Environment Detection Technology Co.LTD, 22 Jinyudadao, 401122, Chongqing, China
[c] Aix-Marseille Univ, CNRS, IRD, INRA, Coll France, CEREGE, 13100, Aix en Provence, France

HIGHLIGHTS

- Negative potential accelerates the start-up speed and enhances the performance of MFCs.
- The higher effluent pH of the MFCs corresponds to a higher COD removal.
- The OC-MFC mode produces the slightest membrane fouling during start-up.
- The abundance of exoelectrogens under the CI-MFC mode is as high as 54.7%.

GRAPHICAL ABSTRACT

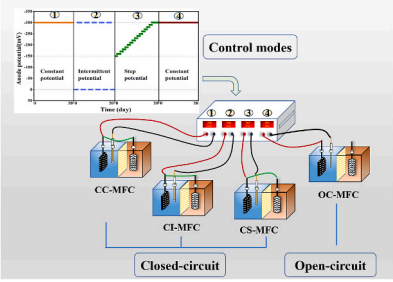

ARTICLE INFO

Keywords:
Wastewater MFC
Anodic potential
Start-up
pH balance
Membrane fouling
Microbial community

ABSTRACT

Wastewater microbial fuel cells (MFCs) can transform the chemical energy into electricity; however, little is known on the effect of circuit modes on start-up and performance of wastewater MFCs. Here we have investigated the effect of four circuit modes on start-up, performance and membrane fouling of MFCs systematically. Besides shortening the start-up period and improving the performance of MFCs, applying anodic negative potential also balances pH of the system and thus enhances COD removal. The open-circuit constant potential mode (OC-MFC) presents the shortest start-up period of 5 days, with the highest voltage output of 810 mV and the slightest membrane fouling, which provides an effectively strategy to accelerate the start-up of wastewater MFCs. The circuit mode applied to start up wastewater MFC not only affects the degree of membrane fouling, but also causes significant differences in anode microbial communities. The total abundance of exoelectrogens in the closed-circuit intermittent potential (CI-MFC) mode was the highest up to 54.70%, but the performance of CI-MFC inferiors to OC-MFC, indicating that performance of the wastewater MFC is not solely determined by the dominant bacteria. Overall, the OC-MFC provides a new strategy to accelerate the start-up period and enhance performance of wastewater MFC simultaneously.

* Corresponding author. 516, Jungong Road, 200093, Shanghai, China.
E-mail address: Liuhb@usst.edu.cn (H. Liu).
[1] Zhenxing Ren and Guixia Ji contribute equally to this work.

Table 1
Comparison of various start-up strategies for microbial fuel cells (MFCs).

MFC type	Start-up strategy	Startup time (days)	Reference
Sediment MFC	The relationship between temperature, pH and voltage was analyzed in detail and the correlation between them was calculated using SPSS software.	/	[43]
Air-cathode MFC	Simultaneous control of the anode potential (−0.2 V) and the external resistance.	40	[44]
Double-chamber MFC	The anode is applied a positive poised potential (+0.2 V) by connecting a potentiostat.	35	[20]
H-type MFC	Gradient based maximum power point tracking (MPPT) and transient poised anode potential followed by MPPT.	20	[45]
Double-chamber MFC	The anode is applied a negative potential (−0.3 V) by connecting a potentiostat.	10	[46]
Sediment MFC	Changing the initial sediment property.	7	[9]
Single chamber MFC	Adding suitable organic substrates (acetate and fumarate).	5	[47]
Single-chamber MFC	Applying transient external voltage (+1 V) application to shorten the start-up time.	4	[48]
Single-chamber MFC	Optimizing the value of the external resistor.	4	[49]
H-type MFC	First-stage preculture and multi-stage MFC reactor-based series culture are used in combination.	1	[50]
Double-chamber MFC	Applying anodic negative potential (−0.3 V) in open circuit mode.	5	This study

/: not explicitly stated.

1. Introduction

Dwindling fossil fuel supplies and increasing energy demand could lead to a global energy crisis [1]. Microbial fuel cells (MFCs) have gained great interest, because of the conversion system utilize chemical energy from wastewater into alternative bioenergy [2]. The conversion is achieved by coupling oxidation reactions that provide electrons at the anode with reduction reactions using electrons at the cathode [3]. These reactions are separated electronically inside the system, forcing electrons to flow through an external circuit, while the movement of ions inside the system maintains charge balance and completes the circuit. As a hybrid bioelectrochemical, different approaches of MFCs have been explored, including electricity generation mechanism [4,5], wastewater treatment [1,2], electrode materials [6], reactor geometry and structure [7], membranes [8], substrate types [9], environmental monitoring [10] and bioremediation [3]. However, biofilm formation is a slow and complex process involving bacterial adhesion to the electrode surface, followed by cell-cell adhesion to form a multilayer biofilm [11]. Consequently, the start-up time of MFC usually takes days to months, limiting its scale application.

Table 1 demonstrates that the start-up period of various wastewater MFCs ranges from 1 to 40 days. Mainly three strategies are used to decrease the start-up period: anodic material modification, cell architecture optimization and application of external potential. Anode is the main location for microbial adhesion and electron transfer from the substrate, whose material composition plays an important role in the performance (e.g., current, power output) and cost of MFCs [12]. Anodic materials modification can improve the biocompatibility and electron mobility to promote the growth of microorganisms. Configurations of MFC vary widely, ranging from single-chamber reactor, to plate and frame (equally sized electrodes) and tubular configurations [13]. Differences in configuration impact the internal resistance and mass transfer efficiency, therefore even when experimental conditions and reactor setups are identical, the biofilm development, MFC performance and start-up time cannot be directly compared [14]. The electrochemical limitations which result from ohmic, kinetic, and transport resistance can be reduced through cell architecture optimization. Anodic potential is a key factor affecting the start-up process, and is directly related to the microbial catalytic activity [15], community composition [16] and metabolic pattern [17]. Growth of microbial biofilms can be induced by precise control of anode potential vs. a reference electrode using potentiostat or DC power supply to apply external power, but the connection to the external power changes the MFC into MEC. Nevertheless, applying a positive or negative anode potential is still under debate [13]. Based on the Gibbs free energy $\Delta G = - n\Delta EF$, where ΔE is the potential difference of electron donor and electron acceptor, F is the Faraday constant, n is the mole of electron transferred. A lower (negative) anodic potential naturally indicates more energy for microbes when the potential is near to NADH reaction potential (−520 mV vs. Ag/AgCl reference electrode) [18]. Another point of view is that positive potential could increase the energy yield per equivalent of substrate oxidation and could accelerate the microbial acclimation [19]; the key exoelectrogens are negatively charged Gram-positive bacteria easier attracted by the positive anodic potential [20].

The separation membranes (e.g., the proton exchange membrane, the cation exchange membrane and the anion exchange membrane) play a crucial role in the performance of wastewater MFCs. The function of a membrane is to transfer protons from the anode to the cathode while preventing the transfer of harmful substances such as oxygen and toxic substrates. Membrane fouling is a major issue that induces physical blockage of charge transfer channels [21]. Chemical fouling is caused by chemicals (e.g., nutrients), present in the liquid media. Chemical fouling occurs mainly on the anodic side of the membrane. Biological fouling refers to membrane pollution by biological processes, e.g., by formation of a biofilm that thickens the membrane and, in turn, increases its resistance to mass transfer and ion transportation [22]. Although researches have recently focused on developing new membrane materials and modifying existing materials to reduce membrane fouling [14,23,24], little is known on the effect of circuit modes on membrane fouling during the start-up of the process.

Therefore, here we studied the effect of four circuit modes, including the closed-circuit constant potential mode (CC-MFC, control), the closed-circuit intermittent potential mode (CI-MFC), the closed-circuit step potential mode (CS-MFC) and the open-circuit constant potential mode (OC-MFC), on the start-up period and cell performance of a wastewater MFC system. Meanwhile, the membrane fouling produced during the start-up stage were measured to reveal the influencing mechanism of circuit modes on membrane fouling. Furthermore, anodic microbial community composition was analyzed to investigate the effect of the circuit modes on the microbial communities. Based on these investigations, we attempt to provide a faster and more effective start-up strategy for the wastewater MFCs.

2. Materials and methods

2.1. Construction of wastewater microbial fuel cells

Four typical two-chamber wastewater MFCs with the same structure were constructed. The reactors were rectangular of 9 × 9 × 12 cm, and the two internal chambers were cylinders of 5 cm in length and 4 cm in diameter, whose working volume of a single chamber is 50 mL. Reactors were screwed in place, whose interface was sealed by a rubber ring and two chambers are separated by a cation exchange membrane (CMI-7000, Membranes International Inc, USA). The anode and cathode are 2 × 3 × 0.2 cm graphite felt and 3 × 3 × 8 cm carbon fiber brush, respectively, both of which are fixed on the top of the reactor, keeping

the distance between the anode and the cathode at 5 cm. The Ag/AgCl reference electrode (SCE,+197 mV *vs* SHE; CHI Co. Ltd, Shanghai, China) was inserted near the anode.

2.2. Inoculation and start-up operations

Anaerobic sludge from the YE Wastewater Treatment Plant, Shanghai, China was used as inoculum, mixed with a 2:3 vol ratio with anode electrolyte. Chemical oxygen demand (COD) of 740 ± 50 mg/L and pH of 6.7 ± 0.1 were measured after centrifugation of the mixture. The anode electrolyte contains 1.64 g $NaCH_3COOH$, 0.31 g NH_4Cl, 4.40 g KH_2PO_4, 3.40 g K_2HPO_4, 0.10 g $CaCl_2{\cdot}H_2O$, 0.10 g $MgCl_2{\cdot}6H_2O$, 12.5 mL trace mineral solution and 5 mL vitamin solution per liter [25]. The anode mixture was aired with nitrogen for 20 min to remove dissolved oxygen before transferred into the anode chamber. The cathode electrolyte was prepared by dissolving 16.64 g $K_3Fe(CN)_6$, 4.40 g $KH_2{\cdot}PO_4$ and 3.40 g $K_2HPO_4{\cdot}3H_2O$ in 1 L deionized water. Solution of two chambers should be changed daily, during which time the poorly adherent bacteria were washed off with 50 mM PBS buffer solution. During the investigation, temperature of all wastewater MFCs was controlled at 25 ± 2 °C, and reactors were homogenized by a magnetic stirrer to eliminate concentration gradients.

The conventional mode of CC-MFC was served as the control group. The MFC was connected to the DC power supply (SPD3303X-E, Siglent Technologies Co. Ltd, America), and kept the anodic potential at − 300 mV *vs* Ag/AgCl in closed circuit by using a wire to connect anode and cathode. The CI-MFC and the CS-MFC modes were connected in the same way as CC-MFC. The CI-MFC was set to apply − 300 mV (*vs* Ag/AgCl) potential to the anode every 1 h. The starting potential of anode in CS-MFC was set to − 150mV (*vs* Ag/AgCl), followed by the applied voltage V_d = - [150 + (D-1) × 10] mV, where D is the number of experimental days, until V_d = - 300 mV, then kept the potential constantly. In the OC-MFC mode, the external circuit of MFC was disconnected and the DC power supply kept the anode potential at −300mV (*vs* Ag/AgCl).

2.3. Electrochemical analysis and calculations

This investigation was conducted for 20 days, and voltage-recovery tests were done on day 5, 12, and 20 compared to the performance between individual MFCs. During the test, MFCs were disconnected from DC power supply, and the voltage between anode and cathode was recorded every 1 min using a data acquisition device (Picolog1216, Pico Technology Inc, UK).

The Coulombic efficiency C_E, an important parameter related to electron transfer efficiency in the whole MFC reaction system, is calculated according to Eq (1).

$$C_E = \frac{M_S \int_0^t Idt}{F b_{es} V_{An} \Delta COD} \tag{1}$$

Where ΔCOD is the substrate concentration variation in one cycle (1 day); t is the cycle time; M_S is the molar mass of the substrate; F is the Faraday constant; V_{An} is the volume of liquid in anode chamber; b_{es} is the amount of transferred electron matter.

Electrochemical tests were measured using electrochemical workstations (CHI 660E, CHI Co. Ltd, Shanghai, China). During tests, the anode of MFC connected to the working electrode while the reference electrode and the cathode connect to the reference electrode and the counter electrode respectively. Polarization and power density curve were obtained by linear sweep voltammetry (LSV) with a scan rate of 1mv/s, using open-circuit potential as the initial and short-circuit potential as the final potential, then obtaining results from the V–I curve. Cyclic voltammetry (CV) can characterize the redox behavior of bioanode. The experiment was operated in three-electrode mode, setting the scan potential range from −0.8 - 0 V with a scan rate of 0.01 mV/s. Before the test of electrochemical impedance spectroscopy (EIS), the external circuit was disconnected for 1 h, setting the open circuit potential as the starting potential, with frequency range of 10^5–10^{-2}Hz, amplitude of 5 mV/s and stabilization time of 100s. The results obtained from the test were fitted in Zview software for analysis.

2.4. Characterization of cation exchange membranes

After the start-up investigations, cation exchange membranes (CEM) were washed with deionized water, to determine the transmittance of four CEM of MFCs in wavenumber range of 600–4000 cm^{-1} using FTIR (Thermo Scientific Nicolet iS5, USA), which was used to identify the variation of functional groups in the CEM under different circuit modes.

The specific proton conductivity (K_M) of CEM was measured to character membrane pollution; two stainless steel electrodes (2 cm apart) were used to provide a constant current and two platinum-wire electrodes (1 cm apart) to record the voltage drop in response to the current supply [26]. The specific proton conductivity (K_M) is calculated by Eq (2), setting potentiostat (CHI 660E, CHI Co. Ltd, Shanghai, China) in the frequency range of 10^5–50 Hz to measure the impedance.

$$K_M = \frac{d}{R_M \times A} \tag{2}$$

Where R_M is the resistance of the membrane; d is the thickness of the membrane; and A is the area of the membrane.

The ion transport number (t_+) is the fraction of the total current carried by a given ion in the electrolyte. We measured t_+ of four cation exchange membranes (single-sided area 12.6 cm^2) in a new reactor equipped with two Luggin capillary reference electrodes (Ag/AgCl) that were placed near the membrane-solution interface to monitor the potential variations. Different concentrations of sodium ions were added to two chambers to drive the concentration gradient [27]; measured electrode potential between the two reference electrodes after 30 min is calculated with Eq (3).

$$E_M = \frac{RT}{F}(2t_+ - 1)\ln\left(\frac{C_1}{C_2}\right) \tag{3}$$

Where E_M is the cell potential (mV); F is the Faraday constant (9.64853 × 104 C); R is the molar gas constant (8.31447 J/mol·K); T is the temperature (K) and t_+ is the transport number of the cation; C_1 and C_2 are the concentrations of electrolytes in different chambers (C_1 = 0.05 mol/L NaCl, C_2 = 0.01 mol/L NaCl).

2.5. Determination of water quality indicators

The chemical oxygen demand (COD) and pH of the influent and effluent were measured daily. COD was measured by a rapid digestion spectrophotometry. 2 mL samples were mixed with digestion solution, then were heated at 150 °C for 2 h in a thermal reactor (DRB200-USA). After samples were cooled, they were measured by spectrophotometry (DR 2800, HACH company, Germany) and recorded averagely of three times. The pH of influent and effluent was measured by a pH meter (FG20, Mettler-Toledo, Switzerland) whose electrode was calibrated using buffers with pH = 4.0 and pH = 6.9 before testing.

2.6. Anode microbial community analysis

For comparative analysis of the bacterial community on anode under different circuit modes, electrodes enriched in microorganisms were collected and immediately stored at −80 °C. According to the manufacturer's protocol, microbial DNA was extracted from the inoculum and electrode samples were prepared using the E.Z.N.A. ® Soil DNA Kit (Omega Bio-tek, Norcross, GA, USA). The V4–V5 regions of the bacterial 16S rRNA gene were amplified by PCR using primers 338F (ACTCCTACGGGAGGCAGCA) and 806R (GGACTACHVGGGTWTCTAAT). PCR

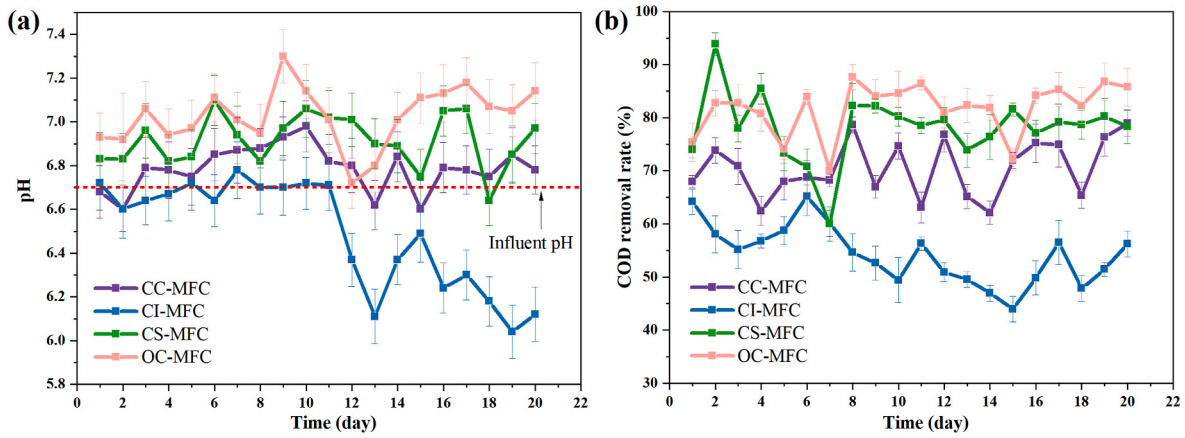

Fig. 1. Variations of effluent pH (a) and COD (b) during 20 days of start-up in MFCs under four circuit modes. The dashed line represents the influent pH.

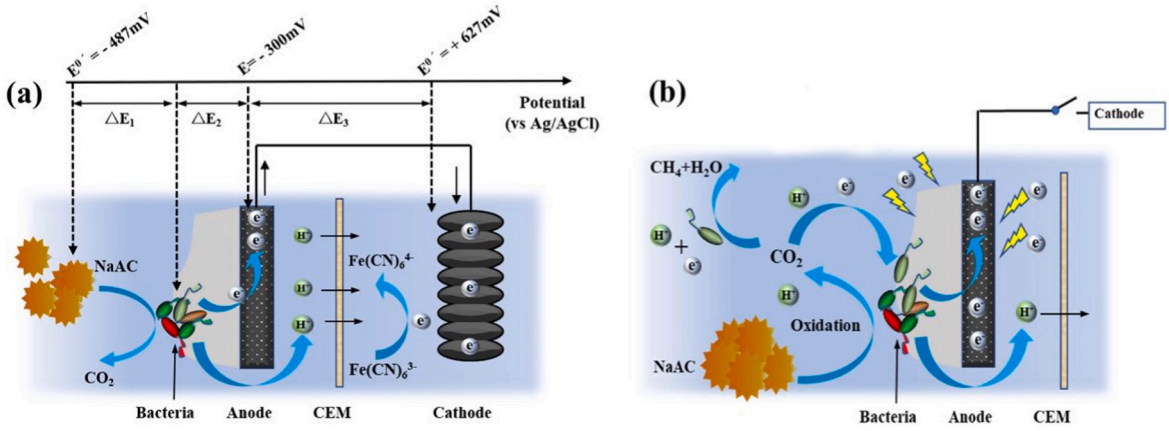

Fig. 2. Tentative mechanism of pH shift of microbial fuel cells (MFC) in closed-circuit (a) and open-circuit (b) conditions. ΔE_1 indicates the potential driving acetate oxidation in Fig. 2a; ΔE_2 represents the potential energy of electron transfer from bacteria to anode, which depended on the energy-saving strategy of the bacteria; ΔE_3 indicates the energy output of MFCs.

was conducted in ABI GeneAmp® 9700 (Applied Biosystems, USA) with the following steps: initial denaturation at 95 °C for 3 min, then denaturing at 95 °C for 30 s, annealing at 55 °C for 30 s, extension at 72 °C for 45 s, and finally extension at 72 °C for 10 min with a total of 27 cycles. After purification and quantification of the PCR products, the microbial communities of anodic biofilms were analyzed using Illumina MiSeq sequencing conducted by Majorbio (Shanghai, China).

3. Results and discussion

3.1. pH balance and substrate degradation

In this study the anodic reaction refers to the oxidation of sodium acetate to CO_2 (Eq (4)) and the cathodic reaction refers to the reduction of ferricyanide (Eq (5)). Typically, in the dual-chamber MFC, due to the generation rate of H^+ exceeds the transfer rate of H^+ with the growth of biofilm, H^+ was accumulated and resulted in the declination of pH at anode, which would affect the microbial activity of subsequent chemical reactions.

$$CH_3COO^- + 2H_2O \rightarrow 2CO_2 + 8e^- + 7H^+ \quad (4)$$

$$Fe(CN)_6^{3-} + e^- \rightarrow Fe(CN)_6^{4-} \quad (5)$$

However, compared with the influent pH, the effluent pH of CC-MFC, CS-MFC and OC-MFC increased during the start-up period (Fig. 1a). The effluent pH of OC-MFC and CS-MFC provided the most noticeable rising. Only the effluent pH of CI-MFC decreased obviously after Day 11. These results suggest that some mechanism may exist to maintain anode pH balance. Fig. 1b demonstrated variations of COD removal rate during 20-day start-up under four circuit modes. All MFCs obtained significantly COD removal rates, with 20-day average COD removal rates of 70.5%, 54.2%, 78.3%, and 81.7% for CC-MFC, CI-MFC, CS-MFC, and OC-MFC, respectively. Interestingly, the COD removal rate showed similar distribution profiles as the effluent pH under four circuit modes, and the COD removal rate of CI-MFC also decreased after Day 11. The higher effluent pH in MFC corresponded to a higher COD removal.

We believe that this pH shift originates from the application of the anodic negative potential. For the closed-circuit mode, an anode potential (E) of −300mV was applied and the energy output of ΔE_3 can reach 927 mV (Fig. 2a), which forces the anodic electrons to reach the cathode quickly and bind to electron acceptors. Simultaneously, more protons were driven through the CEM to participate in the reduction reaction and accelerate the pH balance. The neutral pH is preferred by anodic microorganisms for substrate degradation, and the microbial activity declines at higher or lower pH [28]. Therefore, the pH shift improves the COD removal rate and plays a positive in the closed-circuit mode.

For the open-circuit mode, external negative potential cannot drive protons to the cathode. Another mechanism of pH shift may be occurring (Fig. 2b).

$$CO_2 + 8e^- + 8H^+ \rightarrow CH_4 + 2H_2O \quad (6)$$

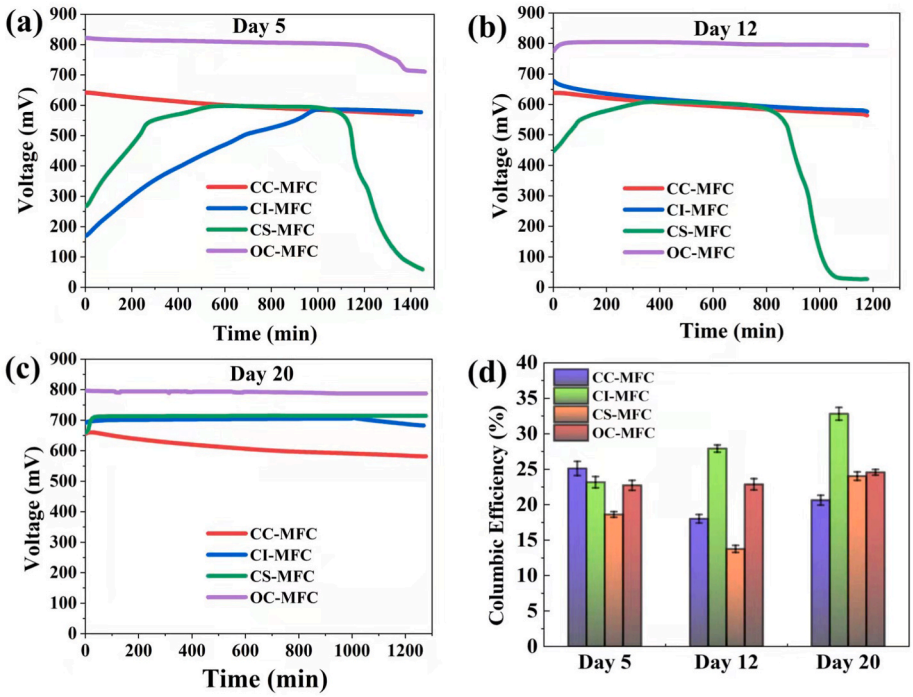

Fig. 3. Voltage-recovery tests on day 5 (a), 12 (b) and 20 (c), and the corresponding coulombic efficiency (d) in different circuit modes.

Acetate acts as the sole electron donator in anode and is metabolized by microorganisms to generate energy and CO_2 (Eq (4)). CO_2 could be captured by anaerobic bacteria to produce CH_4 through directly electron transfer (Eq (6)) [29,30], which reduces the acidity in the anode and thus favors substrate consumption. Besides, the low anodic potential favors biomass production accelerating the growth of microorganisms [15]. In conclusion, the application of negative anode potential is the main factor to promote pH to neutral shift, regardless of closed-circuit or open-circuit mode, thereby enhancing the COD removal rate.

3.2. *Electrochemical performance during start-up*

3.2.1. *Start-up time and coulombic efficiency*

Voltage-recovery tests revealed the difference in electrochemical activity of MFCs in different circuit modes during the start-up stage. As shown in Fig. 3a, although voltage output was generated in both four MFCs on day 5, there was significant difference between them. Compared with the other three MFCs, the OC-MFC generated the highest voltage output and plateaued at 810 mV for about 20h. Furthermore, the OC-MFC reached the maximum voltage level at the beginning, while the CS-MFC and the CI-MFC took longer time (550 and 980 min respectively) to reach the maximum voltage output of 600 mV and 585 mV respectively, Then, their voltage decreased as the substrate concentration decreased, showing a typical bell-shaped curve. These results indicate that the started up of MFC in the open-circuit mode collects exoelectrogens with higher electrochemical activity effectively, with higher electron transfer rate. It can be seen from the voltage-recovery tests on day 12 and day 20 (Fig. 3b and c) that the voltage output of the O-MFC was still 810 mV without a significant increase, but the voltage stabilization time was longer. This is because the bacterial community stabilized partially when the voltage output was stable, while other genus still developed or declined after the voltage stabilization [31]. With the gradual formation of the biofilm, the substrate utilization of the CI-MFC and the CS-MFC also increased continuously. It was noteworthy that although the CC-MFC can generate a high voltage output (about 650 mV) in a short time (5 days), its voltage level could not remain stable after 20 days, indicating that the competition between anode microorganisms is more complex in the closed-circuit constant potential mode, which is not conducive to the exoelectrogens forming predominant genus. According to the results in Fig. 3d, the Coulombic efficiency in CI-MFC remained high in all investigations. Since the Coulombic efficiency was influenced by the competition between exelectrogens and non-exelectrogens on the anode [32], we speculate that CI-MFC favors the growth of exelectrogens.

3.2.2. *Polarization and power density*

Fig. S1 depicted the polarization and power density curve of MFCs in different circuit modes at day 5, 12, and 20. The open circuit voltage (OCV) of OC-MFC stabilized at 500 mV in all polarization tests, which is higher than that of other MFCs. The OCV of CC-MFC, CI-MFC and CS-MFC increased with time, and the slope of their polarization curves decreased gradually, implying the decreasing of polarization resistance and increasing of microbial catalytic activity. On day 20, their OCV were 423 mV, 438 mV and 463 mV respectively. The maximum power density of OC-MFC increased from 15.6 mW/m^2 (day 5) to 25.94 mW/m^2 (day 20). This showed that electrochemical properties of the biofilm are still evolving even after day 5 when the voltage reached a plateau. But the power density of OC-MFC were also higher than other modes at day 5, 12 and 20, presenting the best electrochemical performance. The power density of CI-MFC was increased most significantly, which might be attributed to its highest Coulombic efficiency, with the maximum power density increasing from 0.9 m W/m^2 to 19.1 mW/m^2 in 15 days. In contrast, the power density of CC-MFC increased slowly by 8.1 mW/m^2 in 15 days, which was related to its internal colony competition.

3.2.3. *Electrochemical activity and impedance analysis*

Fig. 4a demonstrated CV curve of the four MFCs before and after start-up in different circuit modes. No visible current generation was observed before the start-up completed. After 20 days of start-up operation, clearly redox peaks were observed. The peaks as current response was considered proportional to the growth of the film. The closed area of CV curve of CC-MFC, CI-MFC, CS-MFC and OC-MFC were 7.6, 8.2, 7.8 and 8.3 times greater after start-up. The oxidation peak potential of the four MFCs were more positive than the applied potential of −300 mV, in agreement with previous studies speculating a self-regulatory strategy of the microbe to obtain higher energy [33]. All four MFCs exhibited

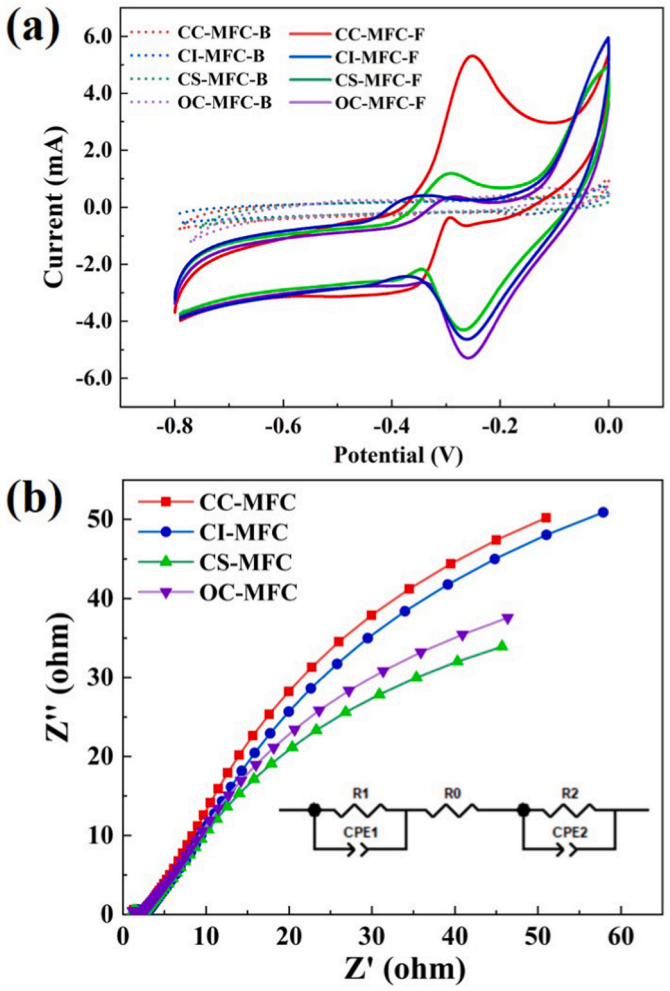

Fig. 4. (a) Cyclic voltammetry (CV) before and after start-up in different circuit modes; (b) Nyquist plots corresponding to the impedance spectra in different circuit modes on day 20.

Table 2
Simulation results of internal resistance in MFC under different circuit modes.

Modes	$R_{total}(\Omega)$	$R_{ohm}(\Omega)$ (R_0)	$R_{trans}(\Omega)$ (R_1+R_2)
CC	51.44	3.64	47.80
CI	58.05	3.12	54.93
CS	46.46	2.60	43.86
OC	45.62	2.52	43.10

oxidation peaks at approximately −0.27 V (*vs* Ag/AgCl), indicating the existence of the same redox species. OC-MFC produced the highest peak current of 5.54 mA, which had high level of redox species. Another oxidation peak of CC-MFC at −0.38 V (*vs* Ag/AgCl) was found, which might be relative to cytochrome Omc B [34]. The reduction peak at −0.26 V (*vs* Ag/AgCl) of CC-MFC was much higher than other peaks, which might be resulted from difference of biofilm performance, allowing more electron-mediated or electroactive enzymes to be produced.

EIS presents the charge transfer impedance on electrode interface, which exhibits a semicircular part in the high frequency region and a linear part in the low frequency region. Fig. 4b showed the Nyquist plots corresponding to the impedance spectra after the completion of the start-up under different circuit modes. The equivalent circuit of Wang et al. was chosen for simulation, where R_0 is the ohmic resistance, R_1 is the anode charge transfer resistance, and R_2 is the cathode charge transfer resistance [20]. The simulation results in Table 2 indicated that the R_{tans} was one order of magnitude higher than the R_{ohm} for each circuit mode, implying that R_{tans} was the main component of R_{toal}. R_{tans} of OC-MFC (13.33 Ω) was smaller than that of CI-MFC, which was equivalent to 3 R_{ohm} of CC-MFC, indicating that the circuit mode had a significant influence on the internal resistance of wastewater MFCs. Although the internal resistance and power density was closely related, there was no absolute linear relationship found. For example, OC-MFC obtained the maximum power density with minimum internal resistance, but the maximum power density of CI-MFC with the biggest internal resistance was slightly lower than that of OC-MFC. Overall, OC-MFC is an effective start-up strategy that not only improves the electrochemical activity of wastewater MFCs, but also reduces the internal resistance.

3.3. *Effect of circuit modes on cation exchange membrane fouling*

After start-up investigations, the fouling of MFC membranes in four circuit modes were evaluated (Fig. 5a). Results showed that the front sides near the anode were more contaminated than the back sides near the cathode. The black fouling appeared higher for the CC-MFC, whereas CI-MFC and OC-MFC modes induced less contamination. We further analyzed residues by FTIR, specific proton conductivity (K_M) and ion transport number (t_+). Fig. 5b contained information on the CEM and the fouling layer. It was observed that characteristic peaks of CEM of all four MFCs appeared below 1500 cm^{-1} with almost identical characteristic peaks obtained, indicating that there was no significant effect of different circuit modes on the functional groups in CEM. The stretching vibration of water (above 1500 cm^{-1}) in CEM of CC-MFC was weaker than in others, due to the difference in membrane performance. The distinctive peaks of sulfonate groups, which are the main functional groups of the CMI-7000 CEM, were observed at 1190 cm^{-1} and 1037 cm^{-1}. The characteristic peak at 1401 cm^{-1} was in the $V_{C=N}$ band associated with the amide group (stretching vibration of the C–N bond), indicating the presence of proteins, and implying the occurrence of microbial fouling of the membrane.

K_M represents the lateral conductivity of membrane, which reflects the condition of membrane fouling. t_+ represents the longitudinal conductivity of the membrane, including the biological fouling covering the membrane surface and chemical fouling. In Fig. 5c, CC-MFC produced the lowest K_M and t_+, implying the heaviest membrane fouling, which is consistent with the observation in Fig. 5a. The OC-MFC performed with K_M and t_+ 6.5 and 2.7 times higher than those of CC-MFC respectively. The difference between CC-MFC and OC-MFC is the circuit mode. Since strong electric field force was applied in CC-MFC, electrons were constantly transferred to cathode to introduce reduction reaction, which allowed cation supporting bacterial transportation across the CEM to maintain charge balance, resulting in blocked ion channel. Some divalent cations (e.g., Mg^{2+}, Ca^{2+}) form precipitates with naturally occurring organic matter in water could create a dense fouling layer on the membrane [35,36], causing chemical contamination. Moreover, multivalent ions can bridge bacterial extracellular polymers, leading to the aggregation and stabilization of biopolymers and microorganisms, resulting in biological fouling [8]. The anode ions in OC-MFC would not be driven by the electric field force to cathode, which greatly reduced the possibility of membrane fouling. Because the potential applied to the anode was stepped up in CS-MFC, the electric field force applied to CS-MFC was smaller than that of CC-MFC, thus the membrane was not contaminated as severely as in CC-MFC. Therefore, it can be concluded that the magnitude and duration of the electric field force during start-up is another important factor affecting the degree of membrane fouling.

3.4. *Anode biofilm microbial community analysis*

The composition of anode microbial community under different

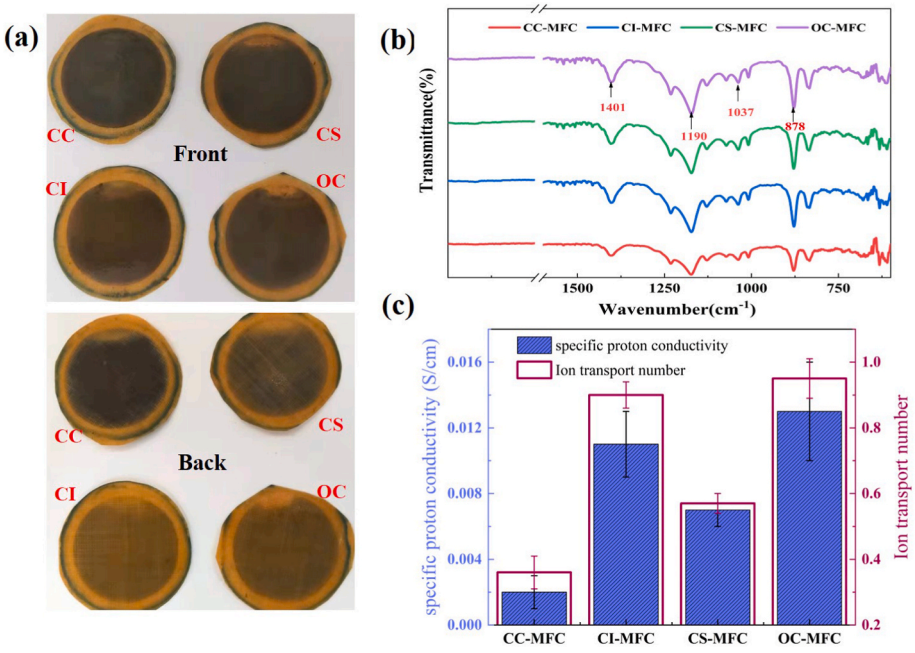

Fig. 5. Analysis of membrane fouling. (a) membrane photos, (b) FTIR spectra of the membranes and (c) characterization of membrane fouling in different circuit modes after 20 days of operation.

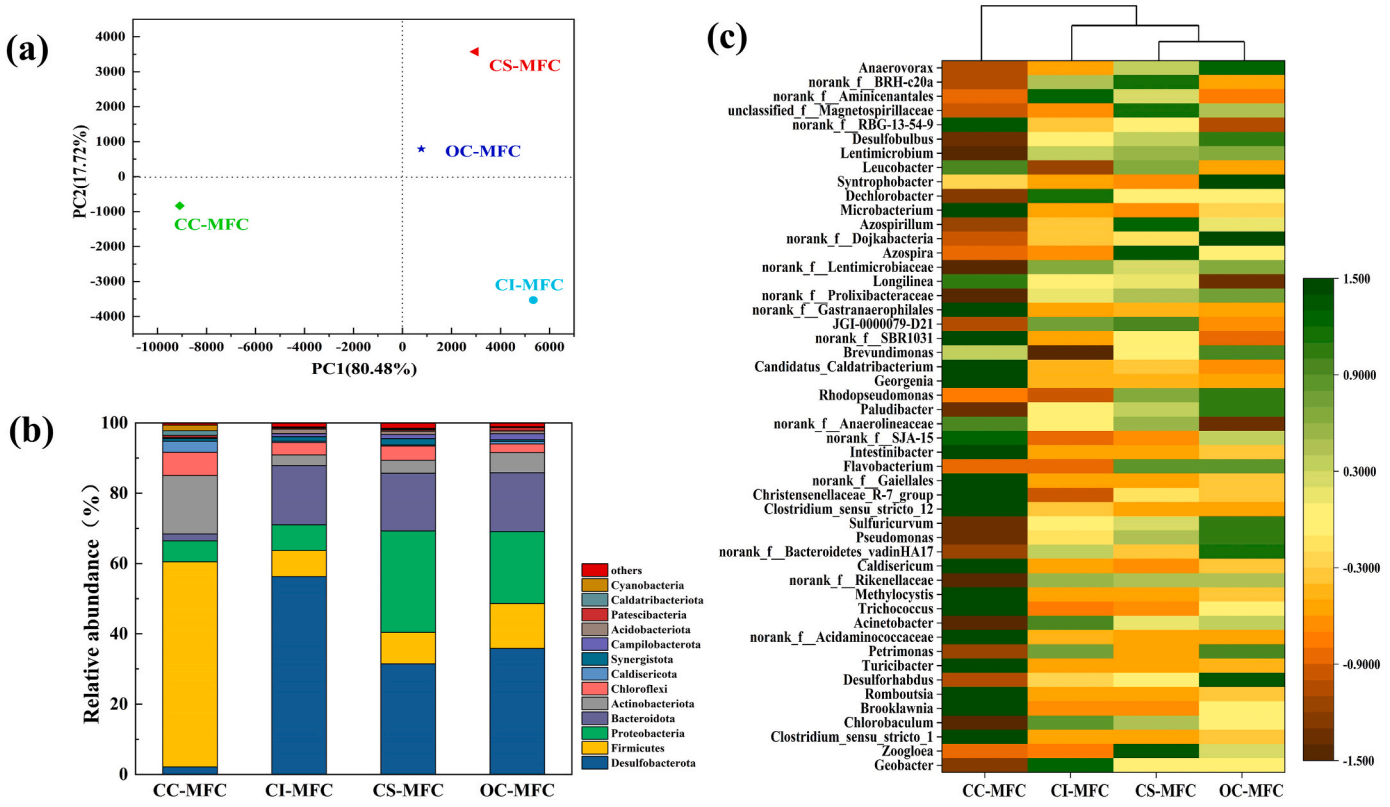

Fig. 6. (a) Principal component analysis on anodic biofilm under four circuit modes; (b) composition and relative abundances in bacterial communities at the phylum level based on 16S rRNA sequences; (c) heatmap of the samples tested for classified bacterial genera with the relative abundance of top 50 illumina sequencing.

circuit modes were analyzed. Table S1 showed the results of Alpha diversity analysis. The Good's coverage of MFCs is generally greater than 0.99, indicating that the sequencing results are reliable. The control group (CC-MFC) presented low abundance but high diversity, showing that the circuit mode made the competitive pressure in anode colony greater than the synergistic effect, which was unsuitable for the development of the dominant colony. The high abundance and diversity of both CS-MFC and OC-MFC implied that the two modes were more

Table 3
Relative abundances of known exoelectrogens in anodic microflora at the genus level based 16S rRNA sequences under four circuit modes (relative abundance ≥ 0.10%).

Samples	Relative abundance (%)				Total (%)
	Geobacter	Pseudomonas	Desulforhabdus	Rhodopseudomonas	
CC	0.11	/	0.10	0.38	0.59
CI	51.35	0.88	2.19	0.28	54.70
CS	26.86	1.31	2.62	0.91	31.70
OC	25.36	1.74	5.89	1.07	34.06

/: not available.

favorable to induce microbial growth. Principal component analysis (PCA) can reflect the similarity of microbial species in different anode biofilm (Fig. 6a), with CS-MFC and CC-MFC both in the upper right quadrant, CI-MFC in the lower right quadrant, and CC-MFC in the lower left quadrant, indicating that different anode microbial species have been developed under different circuit modes, with high similarity between CS-MFC and OC-MFC.

In total, 13 bacterial phyla were identified at the phylum level. As shown in Fig. 6b, *Firmicutes* (58.32%), *Actinobacteriota* (16.63%), *Chloroflexi* (6.59%), and *Proteobacteria* (5.97%) were the dominant bacteria of CC-MFC, and the relative abundance of the minor bacteria *Desulfobacterota* was only 2.15%. Whereas, *Desulfobacterota* was the dominant bacteria of CI-MFC, CS-MFC, and OC-MFC with the relative abundance of 56.31%, 31.44%, and 35.79%, respectively, indicating that different circuit modes caused significant selective variation in the development of anodic microbial community. The relative abundance of *Desulfobacterota* in different modes revealed that it could not be adapted to the strong negative potential condition. *Desulfobacteria* have been reported to be involved in power generation and organic matter degradation and are the main exoelectrogens found in anode biofilm [37]. *Synergistetes* are usually found in acetate-fed MFC, which is used to introduce fermenting bacteria in the anaerobic environment of anode, but with low abundance [38]. *Firmicutes, Chloroflexi* and *Proteobacteria* were the dominant bacteria of CC-MFC, which are also essential for bioelectricity production, such as *Geobacter sulfurreducens*, *Shewanella oneidensis* and *Clostridiumbutyricum EG3* are genera belong to these phyla [39,40]. Therefore, it showed that all four MFC anodes had been adapted to different operating modes and possessed corresponding level of power generation capacity.

We further analyzed anodic biofilm at the genus level, with the 50 dominant genera shown in Fig. 6c. *Geobacter* was the main exoelectrogens of CI-MFC, CS-MFC and OC-MFC. Notably, the highest abundance of *Geobacter* in CI-MFC was 51.35%, indicating that the CI-MFC mode was favorable for the growth and colonization of *Geobacter*. *Geobacter* can provide critical indirect electron transfer without any medium and is one of the most important genera for electron transfer between bacteria and electrodes. A study also indicated that different *Geobacter* evolutionary branches are associated with specific potential [41]. In Table 3, the relative abundance of *Geobacter* in CC-MFC was only 0.11%, together with other known exoelectrogens of *Rhodopseudomonas* (0.38%) and *Desulforhabdus* (0.10%); the total abundance was differed by two orders of magnitude from the CI-MFC (54.70%). However, the electrochemical performance of the CI-MFC mode was not optimal, suggesting that the microbial structural components did not influence the MFC performance directly. Dominant bacteria of *Clostridium_sensu_stricto_1* (21.79%), *Romboutsia* (9.14%), and *Acidaminococcaceae* (5.01%) in CC-MFC all belong to *Firmicutes* phylum, which may be due to the inhibition of the growth of exoelectrogens by the high current of CC-MFC [16]. The abundance of exoelectrogens is grossly inconsistent with electrochemical performance; we speculate that unknown exoelectrogens may be present in CC-MFC. The abundance of *Pseudomonas* in CS-MFC (1.31%) and OC-MFC (1.74%) were similar. *Pseudomonas* are regarded as exoelectrogens responsible for the conversion of VFA into electricity and intermediate compounds, such as phenazine chlorophyll acting as electron shuttles [42].

4. Conclusion

The effect of circuit modes on start-up performance and cation exchange membrane fouling of wastewater MFCs were evaluated in this study. The OC-MFC presented the shortest start-up time of 5 days and the highest voltage output of 810 mV. The degree of membrane fouling was significantly affected by circuit modes and the electric field force; the OC-MFC produced the slightest fouling with specific proton conductivity (K_M) of 0.013 ± 0.003 S/cm and ion transport number (t_+) of 0.954 ± 0.06. Besides, the hypothesis involved in pH balance to enhance substrate (acetate) degradation in anode chamber were proposed. For closed-circuit modes, the application of negative potential in anode produced a high electric field force that accelerates the pH shift to 7.0. For open-circuit modes, anodic pH balance was maintained by side reactions generated by applying negative anode potential, which consumes H^+ to generate biomass and CH_4. The analysis of anode microorganisms demonstrated that microbial community structure varied significantly among four circuit modes, and the total abundance of exoelectrogens in CI-MFC mode was the highest.

CRediT authorship contribution statement

Zhenxing Ren: Investigation, mechanism modelling. **Guixia Ji:** Investigation, Data curation, Supervision. **Hongbo Liu:** Funding acquisition, Conceptualization, Project administration, Supervision, Writing – original draft. **Ming Yang:** Methodology, Data curation. **Suyun Xu:** Writing – review & editing. **Mengting Ye:** Investigation. **Eric Lichtfouse:** Writing – review & editing.

Declaration of competing interest

The authors declare that they have no known competing financial interests or personal relationships that could have appeared to influence the work reported in this paper.

Acknowledgements

The authors have stated that there was no conflict of interest. We gratefully acknowledged the co-funding of this work by the National Natural Science Foundation of China (No.52070130) and the Shuguang Project of Shanghai (Education and Scientific Research Project of Shanghai,18SG45).

Appendix A. Supplementary data

Supplementary data related to this article can be found at https://doi.org/10.1016/j.jpowsour.2022.231403 and below.

References

[1] G. Chen, Electrochemical technologies in wastewater treatment, Separ. Purif. Technol. 38 (2004) 11–41, https://doi.org/10.1016/j.seppur.2003.10.006.

[2] L. Gurreri, A. Tamburini, A. Cipollina, et al., Electrodialysis applications in wastewater treatment for environmental protection and resources recovery: a systematic review on progress and perspectives, Membranes 10 (2020), https://doi.org/10.3390/membranes10070146.

[3] I. Gajda, J. Greenman, C. Melhuish, et al., Water formation at the cathode and sodium recovery using Microbial Fuel Cells (MFCs), Sustain. Energy Technol. Assessments 7 (2014) 187–194, https://doi.org/10.1016/j.seta.2014.05.001.

[4] P. Mandal, M.K. Yadav, A.K. Gupta, et al., Chlorine mediated indirect electro-oxidation of ammonia using non-active PbO2 anode: influencing parameters and mechanism identification, Separ. Purif. Technol. 247 (2020), https://doi.org/10.1016/j.seppur.2020.116910.

[5] G.D. Schrott, P.S. Bonanni, L. Robuschi, et al., Electrochemical insight into the mechanism of electron transport in biofilms of Geobacter sulfurreducens, Electrochim. Acta 56 (2011) 10791–10795, https://doi.org/10.1016/j.electacta.2011.07.001.

[6] Y. Hindatu, M.S.M. Annuar, A.M. Gumel, Mini-review: anode modification for improved performance of microbial fuel cell, Renew. Sustain. Energy Rev. 73 (2017) 236–248, https://doi.org/10.1016/j.rser.2017.01.138.

[7] Y.P. Zhang, J. Sun, B. Hou, et al., Performance improvement of air-cathode single-chamber microbial fuel cell using a mesoporous carbon modified anode, J. Power Sources 196 (2011) 7458–7464, https://doi.org/10.1016/j.jpowsour.2011.05.004.

[8] I.S. Kim, N. Jang, The effect of calcium on the membrane biofouling in the membrane bioreactor (MBR), Water Res. 40 (2006) 2756–2764, https://doi.org/10.1016/j.watres.2006.03.036.

[9] N. Song, H.L. Jiang, Effects of initial sediment properties on start-up times for sediment microbial fuel cells, Int. J. Hydrogen Energy 43 (2018) 10082–10093, https://doi.org/10.1016/j.ijhydene.2018.04.082.

[10] A. Adekunle, V. Raghavan, B. Tartakovsky, A comparison of microbial fuel cell and microbial electrolysis cell biosensors for real-time environmental monitoring, Bioelectrochemistry 126 (2019) 105–112, https://doi.org/10.1016/j.bioelechem.2018.11.007.

[11] Y. Yuan, S.G. Zhou, N. Xu, et al., Microorganism-immobilized carbon nanoparticle anode for microbial fuel cells based on direct electron transfer, Appl. Microbiol. Biotechnol. 89 (2011) 1629–1635, https://doi.org/10.1007/s00253-010-3013-5.

[12] Y. Hindatu, M.S.M. Annuar, A.M. Gumel, Mini-review: anode modification for improved performance of microbial fuel cell, Renew. Sustain. Energy Rev. 73 (2017) 236–248, https://doi.org/10.1016/j.rser.2017.01.138.

[13] R. Rossi, B.E. Logan, Unraveling the contributions of internal resistance components in two-chamber microbial fuel cells using the electrode potential slope analysis, Electrochim. Acta 348 (2020), https://doi.org/10.1016/j.electacta.2020.136291.

[14] L.H. Huang, X.F. Li, Y.P. Ren, et al., Preparation of conductive microfiltration membrane and its performance in a coupled configuration of membrane bioreactor with microbial fuel cell, RSC Adv. 7 (2017) 20824–20832, https://doi.org/ 10.1039/c7ra01014a.

[15] P. Aelterman, S. Freguia, J. Keller, et al., The anode potential regulates the bacterial activity in microbial fuel cells, Commun. Agric. Appl. Biol. Sci. 73 (2008) 85–89.

[16] A. Almatouq, A.O. Babatunde, M. Khajah, et al., Microbial community structure of anode electrodes in microbial fuel cells and microbial electrolysis cells, J. Water Proc. Eng. 34 (2020), https://doi.org/10.1016/j.jwpe.2020.101140.

[17] A. Kumar, A. Siggins, K. Katuri, et al., Catalytic response of microbial biofilms grown under fixed anode potentials depends on electrochemical cell configuration, Chem. Eng. J. 230 (2013) 532–536, https://doi.org/10.1016/j.cej.2013.06.044.

[18] A.J. Wang, W.Z. Liu, N.Q. Ren, et al., Key factors affecting microbial anode potential in a microbial electrolysis cell for H-2 production, Int. J. Hydrogen Energy 35 (2010) 13481–13487, https://doi.org/10.1016/j.ijhydene.2009.11.125.

[19] D. Finkelsein, Effect of electrode potential on electrode-reducing microbiota, Environ. Sci. Technol. (2006).

[20] X. Wang, Y. Feng, N. Ren, et al., Accelerated start-up of two-chambered microbial fuel cells: effect of anodic positive poised potential, Electrochim. Acta 54 (2009) 1109–1114, https://doi.org/10.1016/j.electacta.2008.07.085.

[21] P.N. Venkatesan, S. Dharmalingam, Characterization and performance study on chitosan-functionalized multi walled carbon nano tube as separator in microbial fuel cell, J. Membr. Sci. 435 (2013) 92–98, https://doi.org/10.1016/j.memsci.2013.01.064.

[22] E. Yang, K.J. Chae, I.S. Kim, Assessment of different ceramic filtration membranes as a separator in microbial fuel cells, Desalination Water Treat. 57 (2016) 28077–28085, https://doi.org/10.1080/19443994.2016.1183523.

[23] S. Zinadini, A.A. Zinatizadeh, M. Rahimi, et al., High power generation and COD removal in a microbial fuel cell operated by a novel sulfonated PES/PES blend proton exchange membrane, Energy 125 (2017) 427–438, https://doi.org/10.1016/j.energy.2017.02.146.

[24] S. Kondaveeti, R. Kakarla, H.S. Kim, et al., The performance and long-term stability of low-cost separators in single-chamber bottle-type microbial fuel cells, Environ. Technol. 39 (2018) 288–297, https://doi.org/10.1080/09593330.2017.1299223.

[25] X. Wang, N. Gao, Q. Zhou, Concentration responses of toxicity sensor with Shewanella oneidensis MR-1 growing in bioelectrochemical systems, Biosens. Bioelectron. 43 (2013) 264–267, https://doi.org/10.1016/j.bios.2012.12.029.

[26] R.Q. Fu, J.J. Woo, S.J. Seo, et al., Sulfonated polystyrene/polyvinyl chloride composite membranes for PEMFC applications, J. Membr. Sci. 309 (2008) 156–164, https://doi.org/10.1016/j.memsci.2007.10.013.

[27] M.J. Choi, K.J. Chae, F.F. Ajayi, et al., Effects of biofouling on ion transport through cation exchange membranes and microbial fuel cell performance, Bioresour. Technol. 102 (2011) 298–303, https://doi.org/10.1016/j.biortech.2010.06.129.

[28] S.V. Mohan, Y.V. Bhaskar, P.N. Sarma, Biohydrogen production from chemical wastewater treatment in biofilm configured reactor operated in periodic discontinuous batch mode by selectively enriched anaerobic mixed consortia, Water Res. 41 (2007) 2652–2664, https://doi.org/10.1016/j.watres.2007.02.015.

[29] M. Villano, F. Aulenta, C. Ciucci, et al., Bioelectrochemical reduction of CO2 to CH4 via direct and indirect extracellular electron transfer by a hydrogenophilic methanogenic culture, Bioresour. Technol. 101 (2010) 3085–3090, https://doi.org/10.1016/j.biortech.2009.12.077.

[30] K. Rabaey, W. Verstraete, Microbial fuel cells: novel biotechnology for energy generation, Trends Biotechnol. 23 (2005) 291–298, https://doi.org/10.1016/j.tibtech.2005.04.008.

[31] A. Paitier, A. Godain, D. Lyon, et al., Microbial fuel cell anodic microbial population dynamics during MFC start-up, Biosens. Bioelectron. 92 (2017) 357–363, https://doi.org/10.1016/j.bios.2016.10.096.

[32] D.F. Juang, C.H. Lee, S.C. Hsueh, Comparison of electrogenic capabilities of microbial fuel cell with different light power on algae grown cathode, Bioresour. Technol. 123 (2012) 23–29, https://doi.org/10.1016/j.biortech.2012.07.041.

[33] D.A. Finkelstein, L.M. Tender, J.G. Zeikus, Effect of electrode potential on electrode-reducing microbiota, Environ. Sci. Technol. 40 (2006) 6990–6995, https://doi.org/10.1021/es061146m.

[34] R. Rousseau, M.-L. Délia, A. Bergel, A theoretical model of transient cyclic voltammetry for electroactive biofilms, Energy Environ. Sci. 7 (2014), https://doi.org/10.1039/c3ee42329h.

[35] E. Yang, K.-J. Chae, M.-J. Choi, et al., Critical review of bioelectrochemical systems integrated with membrane-based technologies for desalination, energy self-sufficiency, and high-efficiency water and wastewater treatment, Desalination 452 (2019) 40–67, https://doi.org/10.1016/j.desal.2018.11.007.

[36] D.A. Vermaas, D. Kunteng, M. Saakes, et al., Fouling in reverse electrodialysis under natural conditions, Water Res. 47 (2013) 1289–1298, https://doi.org/10.1016/j.watres.2012.11.053.

[37] W. Liu, A. Wang, D. Sun, et al., Characterization of microbial communities during anode biofilm reformation in a two-chambered microbial electrolysis cell (MEC), J. Biotechnol. 157 (2012) 628–632, https://doi.org/10.1016/j.jbiotec.2011.09.010.

[38] Y.Y. Lee, T.G. Kim, K.S. Cho, Characterization of the COD removal, electricity generation, and bacterial communities in microbial fuel cells treating molasses wastewater, J. Environ. Sci. Health - Part A Toxic/Hazard. Subst. Environ. Eng. 51 (2016) 1131–1138, https://doi.org/10.1080/10934529.2016.1199926.

[39] K. Rabaey, J. Rodriguez, L.L. Blackall, et al., Microbial ecology meets electrochemistry: electricity-driven and driving communities, ISME J. 1 (2007) 9–18, https://doi.org/10.1038/ismej.2007.4.

[40] K. Suzuki, Y. Kato, A. Yui, et al., Bacterial communities adapted to higher external resistance can reduce the onset potential of anode in microbial fuel cells, J. Biosci. Bioeng. 125 (2018) 565–571, https://doi.org/10.1016/j.jbiosc.2017.12.018.

[41] S. Ishii, S. Suzuki, T.M. Norden-Krichmar, et al., Microbial population and functional dynamics associated with surface potential and carbon metabolism, ISME J. 8 (2014) 963–978, https://doi.org/10.1038/ismej.2013.217.

[42] V.N. Srinivasan, C.S. Butler, Ecological and transcriptional responses of anode-respiring communities to nitrate in a microbial fuel cell, Environ. Sci. Technol. 51 (2017) 5334–5342, https://doi.org/10.1021/acs.est.6b06572.

[43] F.Y. Ma, Y.K. Yin, M. Li, Start-up process modelling of sediment microbial fuel cells based on data driven, Math. Probl Eng. (2019), https://doi.org/10.1155/2019/7403732, 2019.

[44] J.M. Haavisto, M.E. Kokko, A.-M. Lakaniemi, et al., The effect of start-up on energy recovery and compositional changes in brewery wastewater in bioelectrochemical systems, Bioelectrochemistry 132 (2020), 107402, https://doi.org/10.1016/j.bioelechem.2019.107402.

[45] H.C. Boghani, J.R. Kim, R.M. Dinsdale, et al., Control of power sourced from a microbial fuel cell reduces its start-up time and increases bioelectrochemical activity, Bioresour. Technol. 140 (2013) 277–285, https://doi.org/10.1016/j.biortech.2013.04.087.

[46] T.Y. Chou, C.G. Whiteley, D.-J. Lee, et al., Control of dual-chambered microbial fuel cell by anodic potential: implications with sulfate reducing bacteria, Int. J. Hydrogen Energy 38 (2013) 15580–15589, https://doi.org/10.1016/j.ijhydene.2013.04.074.

[47] G. Liu, M.D. Yates, S. Cheng, et al., Examination of microbial fuel cell start-up times with domestic wastewater and additional amendments, Bioresour. Technol. 102 (2011) 7301–7306, https://doi.org/10.1016/j.biortech.2011.04.087.

[48] M. Sun, Z.-X. Mu, G.-P. Sheng, et al., Effects of a transient external voltage application on the bioanode performance of microbial fuel cells, Electrochim. Acta 55 (2010) 3048–3054, https://doi.org/10.1016/j.electacta.2010.01.020.

[49] G. Buitrón, I. López-Prieto, I.T. Zúñiga, et al., Reduction of start-up time in a microbial fuel cell through the variation of external resistance, Energy Proc. 142 (2017) 694–699, https://doi.org/10.1016/j.egypro.2017.12.114.

[50] H. Lu, Y. Yu, H. Xi, et al., A quick start method for microbial fuel cells, Chemosphere 259 (2020), 127323, https://doi.org/10.1016/j.chemosphere.2020.127323.

Supplementary material

Accelerated start-up and improved performance of wastewater microbial fuel cells in four circuit modes: role of anodic potential

Zhenxing Ren[1a], Guixia Ji[1a], Hongbo Liu[*a], Ming Yang[b], Suyun Xu[a], Mengting Ye[a], Eric Lichtfouse[c]

a School of Environment and Architecture, University of Shanghai for Science and Technology, 516 Jungong Road, 200093, Shanghai, China. b Chongqing New World Environment Detection Technology Co.LTD, 22 Jinyudadao, 401122, Chongqing, China. c Aix-Marseille Univ, CNRS, IRD, INRA, Coll France, CEREGE, 13100 Aix en Provence, France

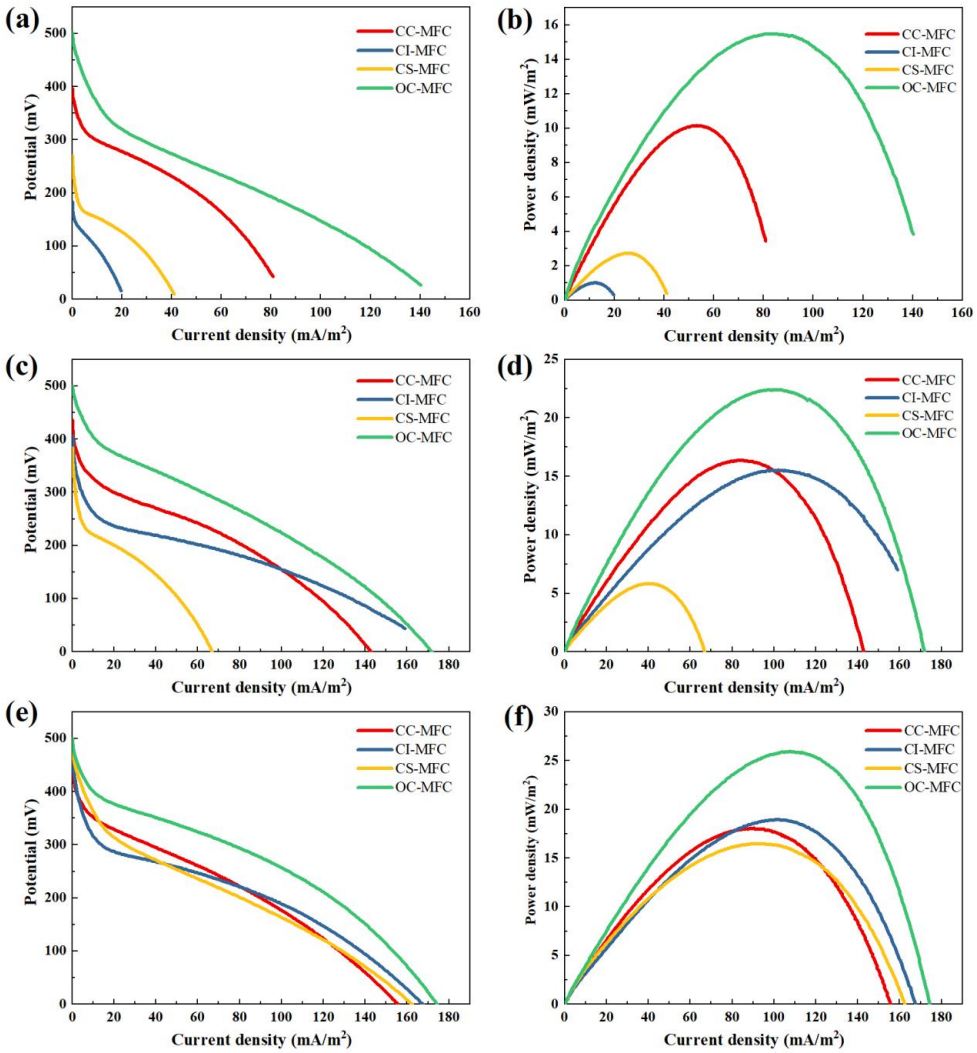

Figure S1. Polarization curves of day 5 (a), 12 (c), 20 (e) and power density curves of day 5(b), 12 (d), 20(f) in different circuit modes.

Table S1. The results of Alpha diversity analysis of MFC in four circuit modes.

Samples	Ace	Chao	Shannon	Simpson	Good's coverage
CC	607.79	594.16	3.95	0.048	0.99681
CI	715.58	706.37	3.21	0.185	0.99375
CS	731.71	707.56	3.73	0.083	0.99578
OC	723.32	718.13	3.98	0.065	0.99485

* Corresponding author post address: 516, Jungong Road, 200093, Shanghai, China;
Email: Liuhb@usst.edu.cn (H., Liu)
Tel: +86(21)55275979; Fax: +86(21)55275979
1 Zhenxing Ren and Guixia Ji contribute equally to this work